

AD-A070 947

RICE UNIV HOUSTON TEX

F/G 4/1

STUDY TO ANALYZE AND SYNTHESIZE SATELLITE DATA.(U)

JAN 79 M HAREL, P H REIFF, R W SPIRO

F19628-78-C-0078

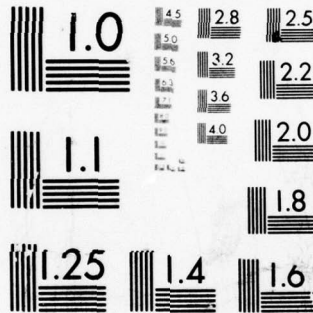
UNCLASSIFIED

AFGL-TR-79-0024

NL

/ OF 1
AD A070 947





MICROCOPY RESOLUTION TEST CHART
NATIONAL BUREAU OF STANDARDS-1963-A

12 LEVEL II

AFGL-TR-79-0024

STUDY TO ANALYZE AND SYNTHESIZE SATELLITE DATA

M. Harel
P. H. Reiff
R. W. Spiro
R. A. Wolf

William Marsh Rice University
6100 S. Main Street
Houston, Texas 77005

Final Report
1 October 1977 - 30 September 1978

15 January 1979

Approved for public release; distribution unlimited

ADA 070947

DDC FILE COPY

AIR FORCE GEOPHYSICS LABORATORY
AIR FORCE SYSTEMS COMMAND
UNITED STATES AIR FORCE
HANSCOM AFB, MASSACHUSETTS 01731

DDC
RECEIVED
JUL 10 1979
B

305 750

79 07 09 004

Qualified requestors may obtain additional copies from the Defense Documentation Center. All others should apply to the National Technical Information Service.

REPORT DOCUMENTATION PAGE		READ INSTRUCTIONS BEFORE COMPLETING FORM
1. REPORT NUMBER 19 AFGL-TR-79-0024	2. GOVT ACCESSION NO.	3. RECIPIENT'S CATALOG NUMBER
4. TITLE (and Subtitle) Study to Analyze and Synthesize Satellite Data		5. TYPE OF REPORT & PERIOD COVERED Final Report 1 Oct 1977 - 30 Sept 1978
7. AUTHOR(s) M. Harel, P. H. Reiff, R. W. Spiro and R. A. Wolf		6. PERFORMING ORG. REPORT NUMBER
9. PERFORMING ORGANIZATION NAME AND ADDRESS William Marsh Rice University 6100 S. Main Street Houston, Texas 77005		8. CONTRACT OR GRANT NUMBER(s) F19628-78-C-0078
11. CONTROLLING OFFICE NAME AND ADDRESS Air Force Geophysics Laboratory Hanscom AFB, Massachusetts 01731 Contract Monitor: Michael Smiddy (PHG)		10. PROGRAM ELEMENT, PROJECT, TASK AREA & WORK UNIT NUMBERS 61102F 231162AS
14. MONITORING AGENCY NAME & ADDRESS (if different from Controlling Office)		12. REPORT DATE 15 January 1979
		13. NUMBER OF PAGES 33
		15. SECURITY CLASS. (of this report) Unclassified
16. DISTRIBUTION STATEMENT (of this Report): Approved for public release; distribution unlimited.		
17. DISTRIBUTION STATEMENT (of the abstract entered in Block 20, if different from Report):		
18. SUPPLEMENTARY NOTES		
19. KEY WORDS (Continue on reverse side if necessary and identify by block number) Magnetosphere Ring Current Ionosphere Electric Fields Substorm		
20. ABSTRACT (Continue on reverse side if necessary and identify by block number) We have completed four computer runs simulating the behavior of the earth's inner magnetosphere during the substorm-type event that had its onset at about 1000 UT on 19 September 1976. Our program simulated many aspects of the behavior of the closed-field-line portion of the auroral and subauroral ionosphere. For these regions, the program self-consistently computes electric fields, electric currents, hot-plasma densities, plasma flow velocities and other parameters.		

D D C
RECEIVED
 JUL 10 1979
RECEIVED
 B

305 750

Our computed ionospheric electric fields compare reasonably well with corresponding data from satellite S3-2. The most striking observational feature of the electric fields in the modeled region during the 19 September 1976 event was an instance of rapid subauroral flow, which was observed on the outbound part of pass 4079B South and was also predicted by the computer runs. These computer results seem consistent with a simple analytic model for rapid subauroral flow developed by Southwood and Wolf.

Birkeland-current densities predicted by the model are presented, for eventual comparison with S3-2 magnetometer data.

A program has been developed to follow the evolution of the plasmasphere, or any other magnetospheric or upper-ionospheric cold-plasma boundary, through a modeled event. Some interesting preliminary results for computed plasmasphere shapes are presented.

TABLE OF CONTENTS

I. Contract Tasks 1

II. Scientific Results..... 2

 A. Time Evolution of the Plasmopause..... 2

 B. Ionospheric Conductivity..... 9

III. Business Data 9

 A. Contributing Scientists..... 9

 B. Previous and Related Contracts.....10

 C. Publications.....10

 D. Travel.....11

 E. Personnel Changes.....11

 F. Property Acquired.....11

 G. Additional Information.....11

 H. Fiscal Information.....11

 I. Cumulative Cost Data.....11

Appendix, Comparison of Model Predictions with
Data from Satellite S3-2.....12

Accession For	
NTIS GRA&I	<input checked="" type="checkbox"/>
DDC TAB	<input type="checkbox"/>
Unannounced Justification	<input type="checkbox"/>
By _____	
Distribution/ _____	
Availability Codes	
Dist.	Avail and/or special
A	

I. CONTRACT TASKS

Analyze and synthesize data from the Air Force S3-2 and S3-3 satellites at different altitudes to establish proper boundary conditions for present and future models. Perform multiple runs of existing computer models to find the optimum fit of the model to the satellite data. Make a detailed comparison between the optimized computer simulation and the data. Refine estimated integrated ionosphere conductivity using DMSP photographs and electron spectrometer data, simultaneous Chatanika data and S3-2/S3-3 observations and implement these estimates into computer simulation.

II. SCIENTIFIC RESULTS

We have completed and thoroughly analyzed results of four simulation runs for the event of 19 September 1976, and have made detailed comparisons with S3-2 data. These results are presented in Appendix I

Two other aspects of the work have not been written up in detail for journal articles, but should be described briefly here. They are (A) the problem of modeling the time-evolution of the plasmopause; (B) the problem of modeling height-integrated ionospheric conductivity.

A. Time Evolution of the Plasmopause

R. W. Spiro has developed a program that integrates ExB-drift velocities to trace the motion of flux tubes of low-energy plasma through the magnetosphere during the simulated event. By assuming an initial plasmopause shape at the beginning of the event, and following the trajectories of many particles from that initial boundary, through the simulated event, we have predictions as to the time history of the plasmopause through the event.

Results from one of these sets of calculations are shown in Figures 1-5. These results are for the simulation run that is expected to be the most accurate (Run #4 in Table 1 of Appendix I), although similar calculations have been carried out for Runs 1-3 also. Figure 1 shows the initial assumed plasmopause, based on the last closed equipotential for the potential distribution at 0900UT, before the growth phase of the substorm. Figures 2-5 show the computed plasmopause shapes at various times during the event. The most interesting result is the formation of two long plasmatails (or "regions of detached plasma") during the one simulated event. (Previous calculations, using simpler electric-field configurations (e.g., Chen and Wolf, *Planet. Space Sci.*, 20, 483, 1972; Grebowsky, *JGR*, 71, 6193, 1971) did not predict multiple plasmatails for simple single-substorm events. In the simulation of the 19 September 1976 event, the second plasmatail forms during the period of increasing convection electric field; during such a period, there is a significant eastward electric field at $L \approx 5$, just past local dusk (see Figure 6); this eastward field kicks plasmasphere flux tubes out away from the earth, into the stream that is flowing rapidly sunward, outside the shielding layer. The result is formation of a plasmatail that extends toward the dayside magnetosphere from a base in the plasmasphere near dusk.

NO. 14 12-20-78; CASE=NR; INIT=SAD-1.

TIME = 9.15

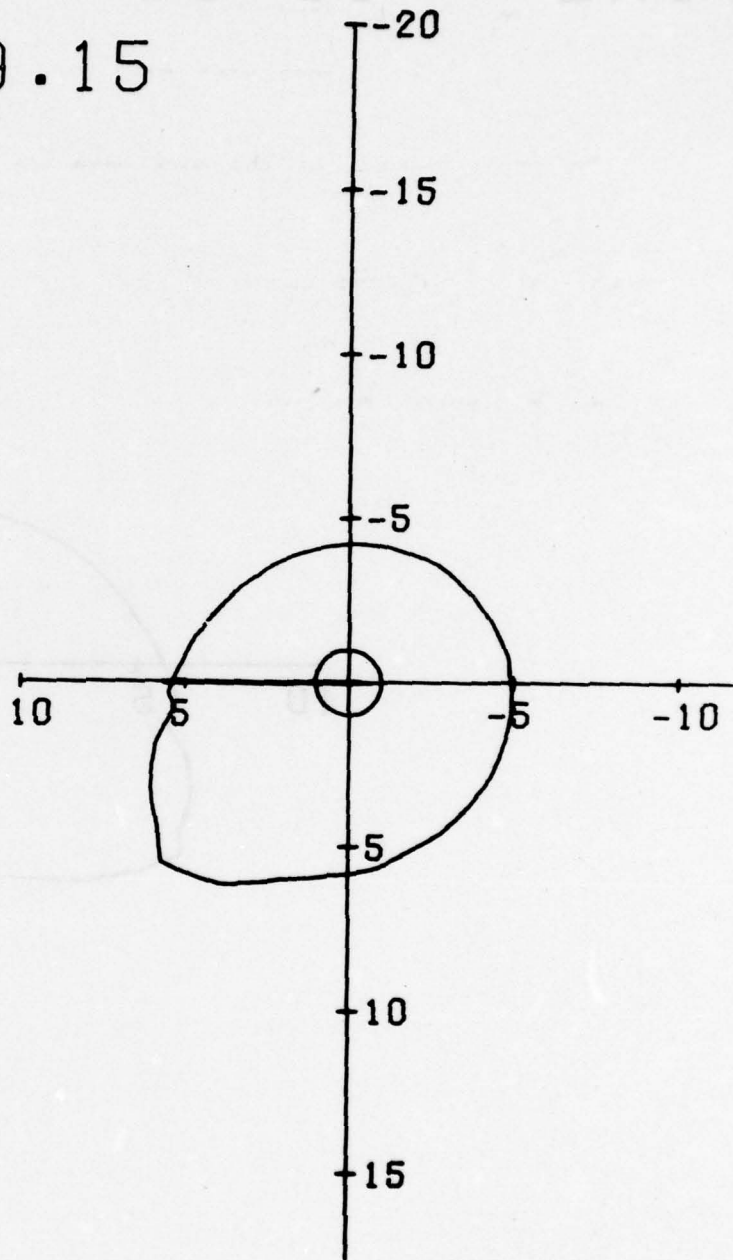


Figure 1

Configuration of the plasmopause, in the magnetospheric equatorial plane, for 0915 UT on 19 September 1976. The sun is to the left.

NO. 18 12-20-78; CASE=NR; INIT=SAD-1.

TIME = 10.00

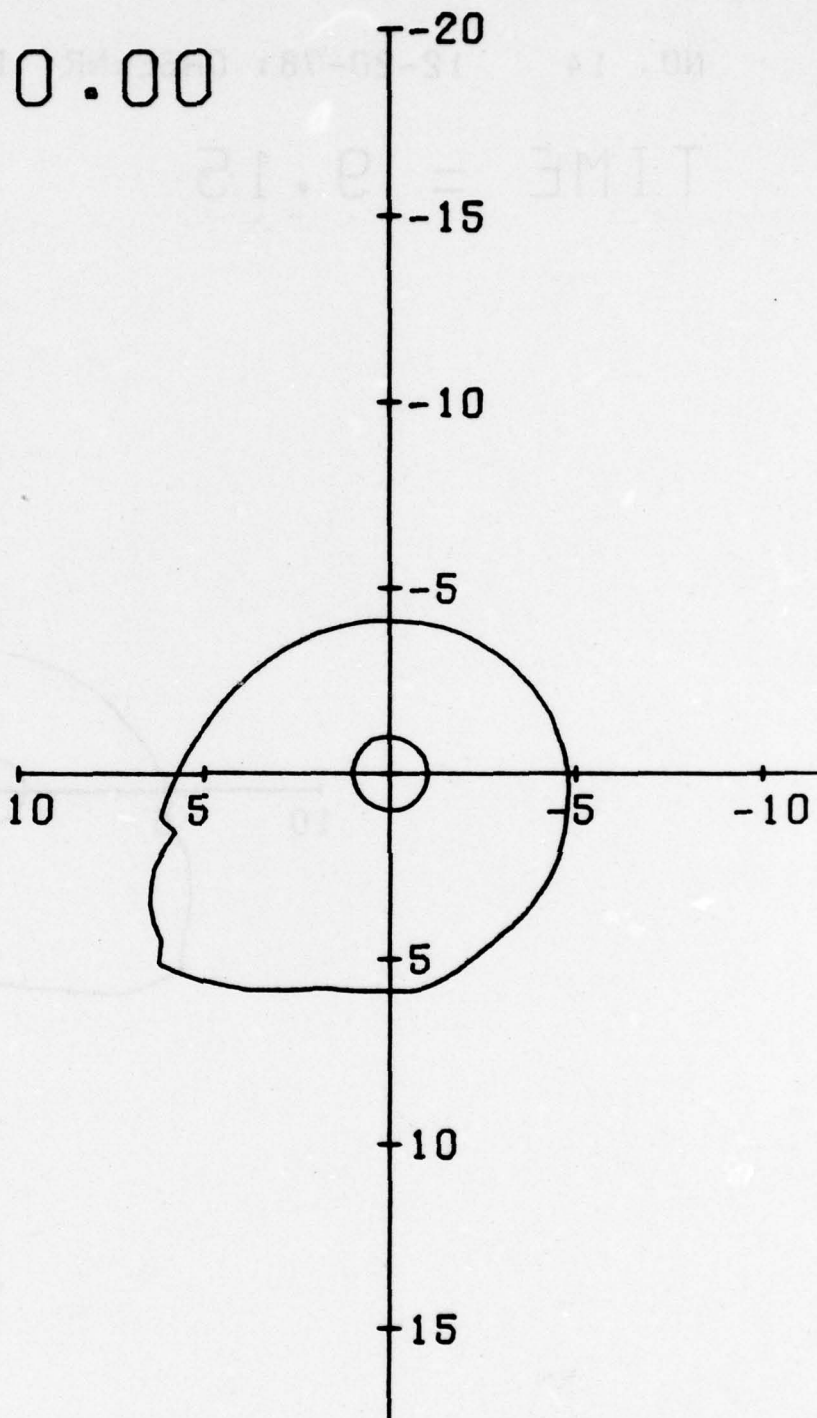


Figure 2

Plasmopause configuration for 1000 UT on
19 September 1976.

NO. 2 12-20-78; CASE=NS; INIT=SAD-1.

TIME = 11.00

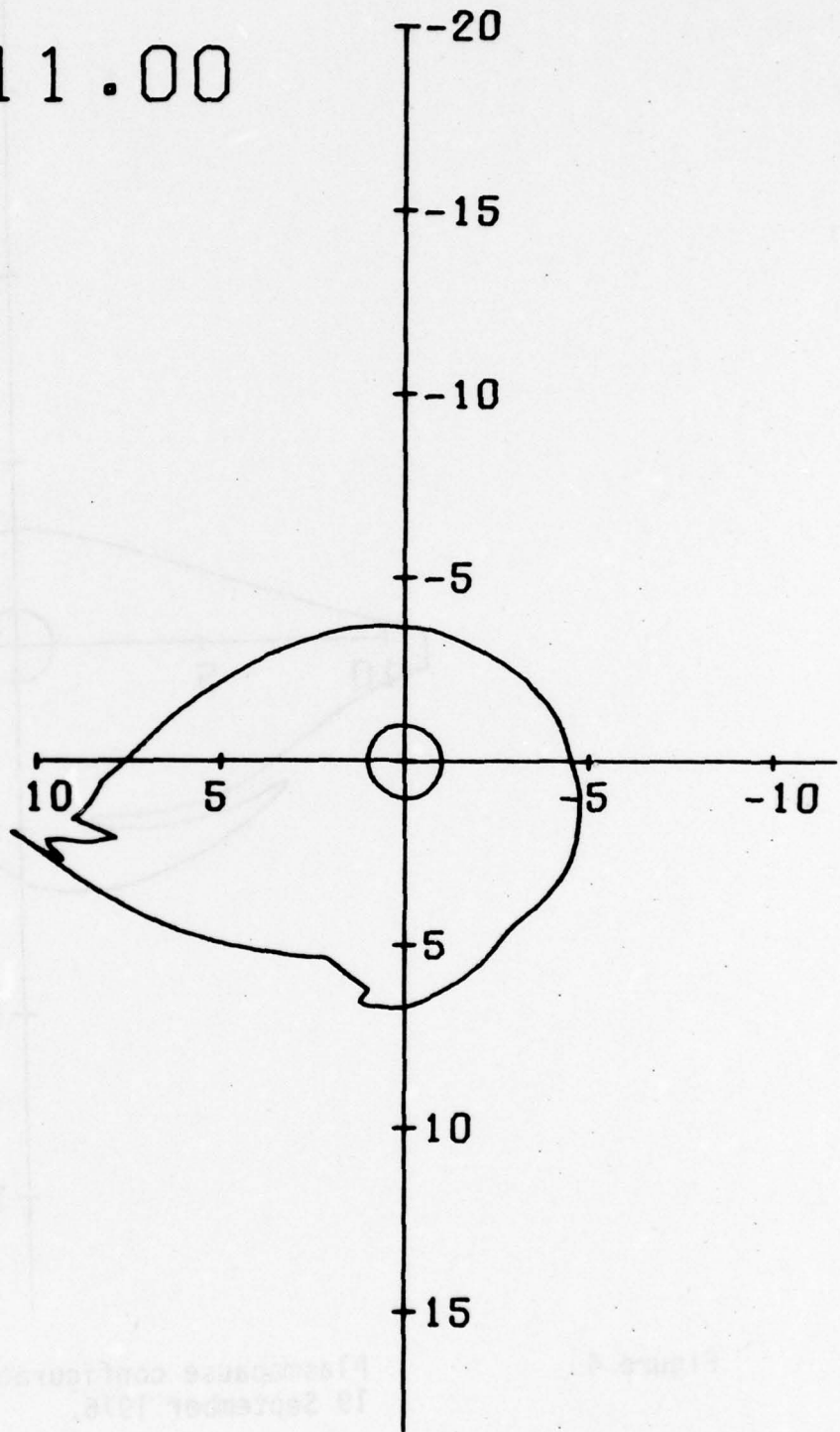


Figure 3

Plasmopause configuration for 1100 UT on
19 September 1976.

NO. 8 12-20-78; CASE=NS; INIT=SAD-1.

TIME = 12.00

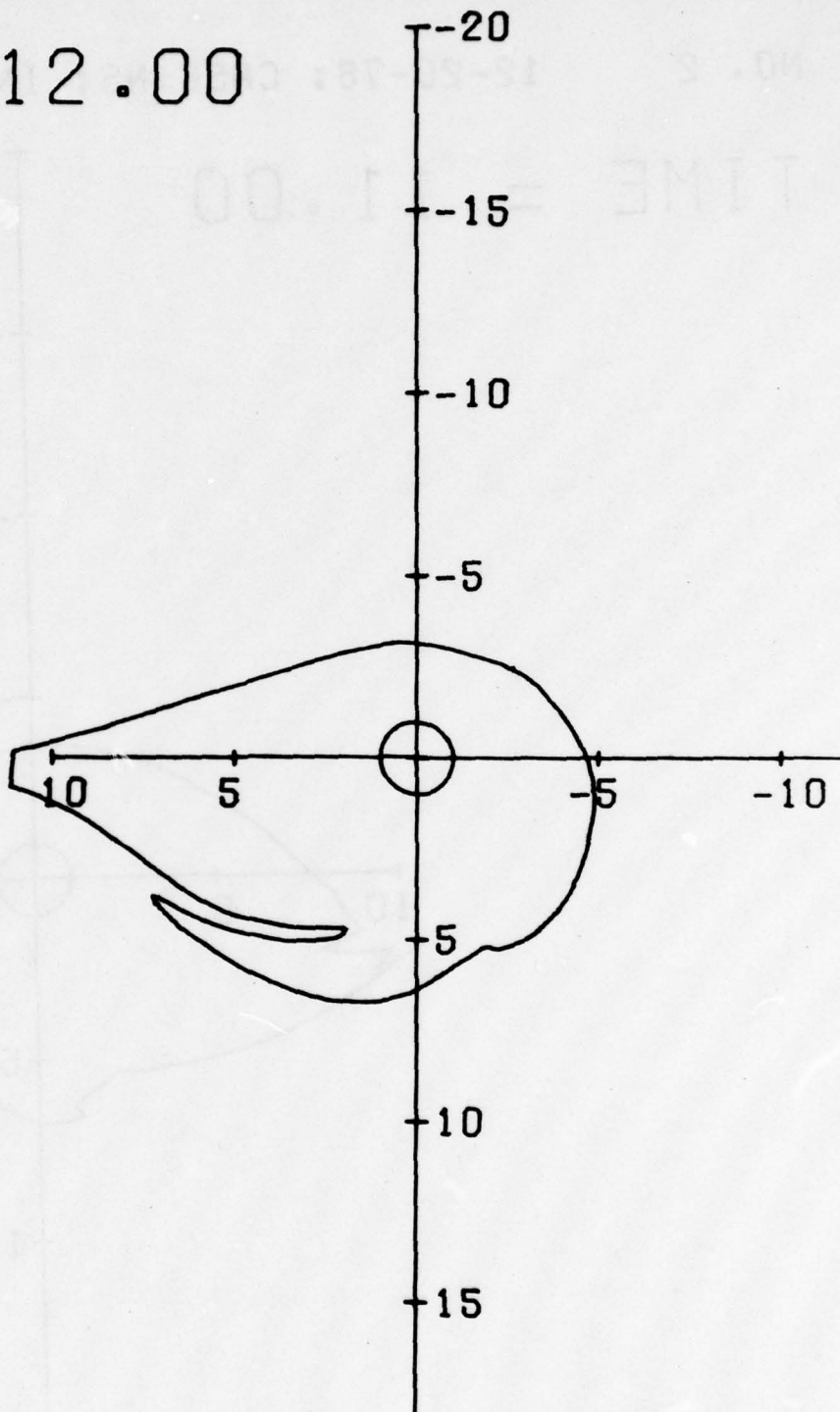


Figure 4

Plasmopause configuration for 1200 UT on
19 September 1976.

NO. 14 12-20-78; CASE=NS; INIT=SAD-1.

TIME = 13.00

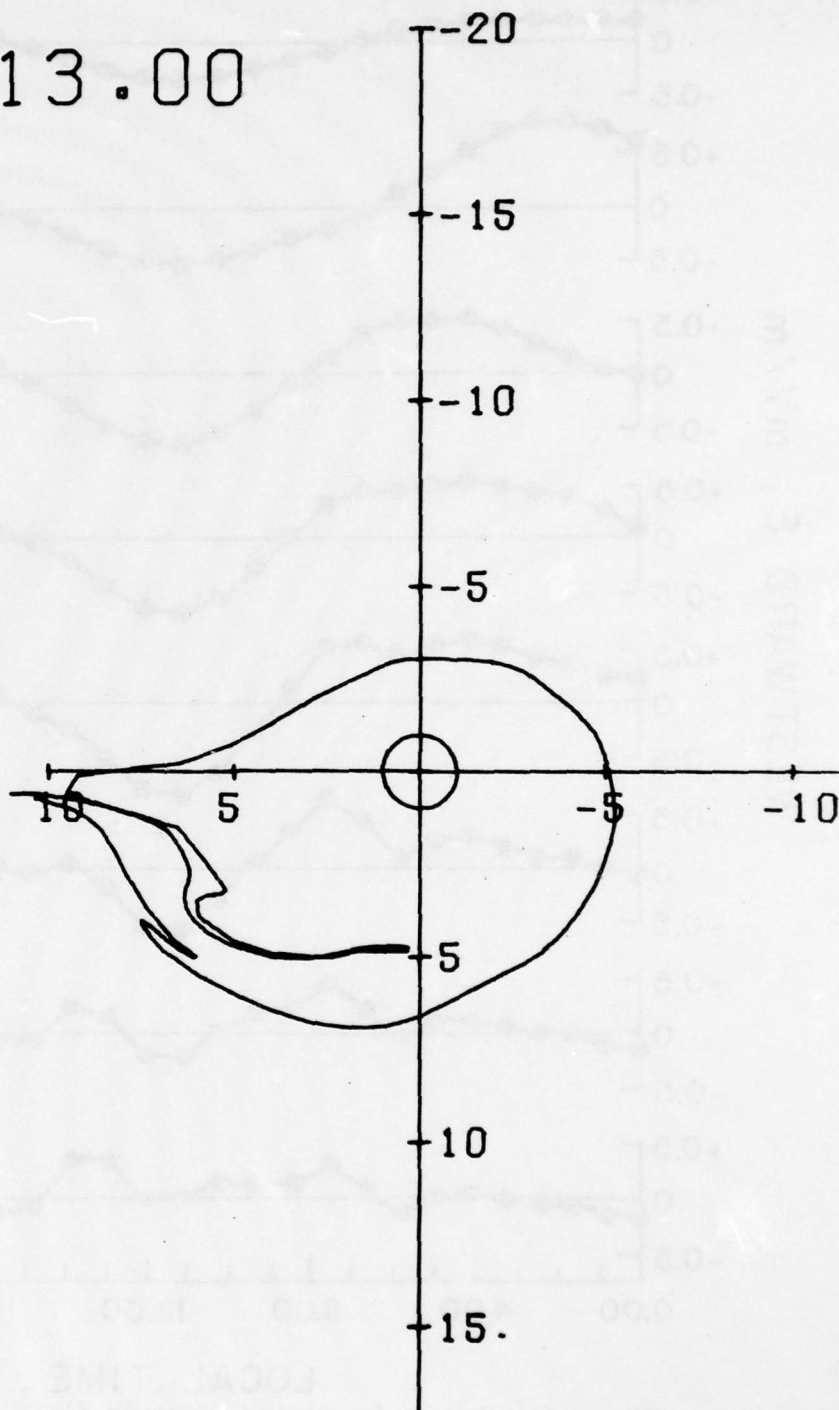


Figure 5

Plasmopause configuration for 1300 UT on
19 September 1976.

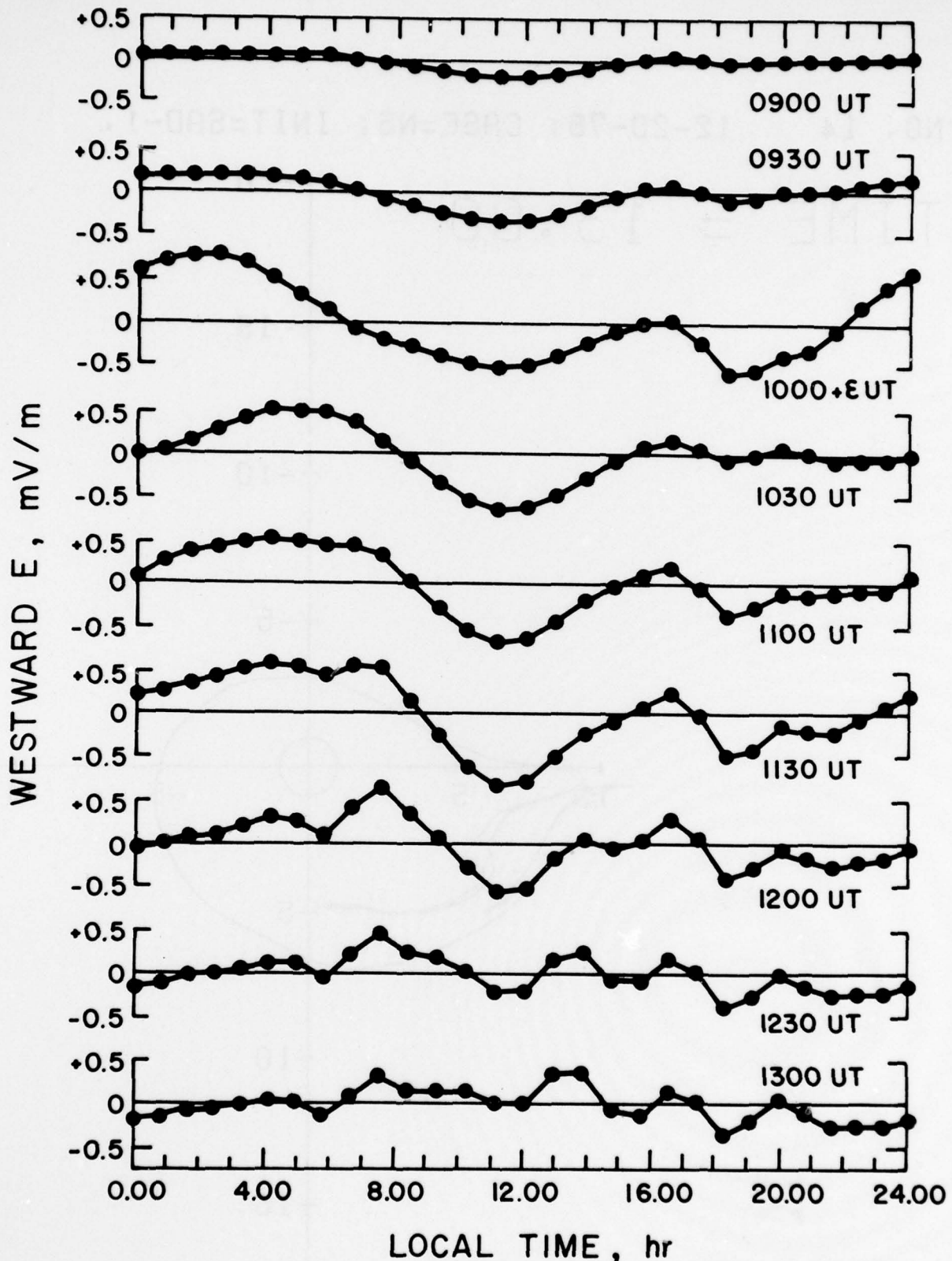


Figure 6 Computed westward electric field, in the magnetospheric equatorial plane, for 19 September 1976 at $L \approx 4.6$.

Similar time-sequence plots have been obtained for the other 3 computer runs. This second tail forms in all cases, although in some cases a shorter third tail is also present. The final configuration is found not to be sensitively dependent on the assumed initial size of the plasmasphere.

B. IONOSPHERIC CONDUCTIVITY

The least successful part of this first event simulation has been the part dealing with the model for height-integrated conductivity.

It now appears that the best approach to obtaining a time-dependent model of auroral enhancement of height-integrated ionospheric conductivity for a simulated event is the following: (1) use electron fluxes measured from polar-orbiting satellites and approximate empirical formulas to devise auroral enhancement of height-integrated Pedersen and Hall conductivities (see AFGL report TR-77-0286) along the subsatellite track; (2) use DMSP photos to estimate very roughly the local-time dependence of the enhancements. When available, data from Chatanika radar can be used to supplement measured electron fluxes and improve accuracy.

In the four simulations done so far for the 19 September 1976 event, we encountered several serious difficulties: (i) for this event, we relied heavily on electron detectors from satellite S3-2 for data of type (1); unfortunately, electron fluxes in the diffuse aurora are close to the instrument noise level, and we were not able to get really trustworthy estimates of conductivity enhancements along the subsatellite track in the diffuse aurora; (ii) we found that our numerical method of representing the current-conservation equation in the ionosphere by a difference equation was not trustworthy in regions of sharp conductivity gradients; sharp latitudinal jumps in conductivity had to be blurred out over $\sim 2^\circ$ to make the numerical method reliable.

To solve these problems, we plan to choose future events for simulation with an eye toward availability of J/3 data from DMSP satellites, or of similar high-sensitivity electron-flux data from some other source. We also plan to seek an improved ionospheric difference equation that will behave better in the presence of sharp conductivity gradients.

III. BUSINESS DATA

A. Contributing Scientists

Rice University

A. Ahmad, Graduate Student Programmer

M. Harel, Scientist I

H. K. Hills, Senior Research Associate

J. L. Karty, Summer Assistant
P. H. Reiff, Assistant Professor
R. W. Spiro, Research Associate
R. A. Wolf, Professor

AFGL

M. Smiddy
D. A. Hardy

Regis College

W. J. Burke
F. J. Rich

B. Previous and Related Contracts

F19628-77-C-0012 (10/01/76 - 9/30/77)

F19628-77-C-0005 (10/01/76 - 9/30/79)

C. Publications

Harel, M., R.A. Wolf and P. H. Reiff, Results of computer simulating the inner magnetosphere during a substorm-type event, in Magnetosphere, Contributed Papers presented at the Solar-Terrestrial Physics Symposium, Innsbruck, 1978.

Harel, M., R. A. Wolf, P.H. Reiff and M. Smiddy, Computer Modeling of events in the inner magnetosphere, to be published in Quantitative Modeling of the Magnetospheric Processes, Geophys. Monogr. Ser., Vol 21 edited W. P. Olson, AGU, Washington, D.C., 1979.

Papers Presented at Meetings

Reiff, P.H., R. A. Wolf and M. Smiddy, Substorm variations of the polar-cap potential drop, presented at the AGU meeting, Miami Beach, April, 1978.

Harel, M., R.A. Wolf, H.K. Hills and A.C. Calder, Computer model for simulating the inner magnetosphere during a substorm, presented at the AGU meeting, Miami Beach, April, 1978.

Wolf, R.A., M. Harel and P.H. Reiff, Comparison of preliminary results of substorm computer simulation with observational data, presented at the AGU meeting, Miami Beach, April 1978.

Harel, M., R.A. Wolf and P.H. Reiff, Results of computer simulating the inner magnetosphere during a substorm-type event, presented at the COSPAR meeting, Innsbruck, Austria, 1978.

Harel, M. R. A. Wolf, P.H. Reiff and M. Smiddy, Computer modeling of events in the inner magnetosphere, presented at the Chapman Conference on Quantitative Modeling of Magnetospheric Processes, La Jolla, Ca., September, 1978.

D. Travel Performed

R. A. Wolf attended the spring AGU meeting in Miami Beach and presented one of a series of three papers describing results of the first simulation. He also attended the quantitative modeling in La Jolla and presented a paper giving later results. Part of the incumbent travel expenses were paid from this contract.

E. Personnel Changes

H. K. Hills, Co-investigator, left Rice in July, 1978 to work at the National Space Science Data Center. Professor P. H. Reiff put extra effort into the contract, and Dr. Hills' departure did not disrupt work.

F. Property Acquired

None

G. Additional Information

None

H. Fiscal Information

Of the total of \$25,000 for this contract, essentially 100% has been expended. The work required under the contract has been completed.

I. CUMULATIVE COST DATA

<u>Elements</u>	<u>Amount Planned</u>	<u>Actual</u>
<u>Labor</u>		
Principal Investigator and Co-Investigator	\$ 8,473	\$3,494
Other Faculty, Staff & Students	4,468	9,365
<u>TOTAL LABOR</u>	<u>\$12,941</u>	<u>\$ 12,859</u>
<u>Direct Nonlabor Expenses</u>		
Travel	\$ 1,100	\$ 444
Computing	1,000	1,803
<u>Other expenses</u>	<u>2,453</u>	<u>2,428</u>
<u>TOTAL DIRECT EXPENSES</u>	<u>\$4,553</u>	<u>\$ 4,675</u>
Overhead	\$7,506	\$ 7,459
<u>GRAND TOTAL</u>	<u>\$25,000</u>	<u>\$ 24,993</u>

**APPENDIX: COMPARISON OF MODEL PREDICTIONS WITH
DATA FROM SATELLITE S3-2**

M. Harel, R. A. Wolf and P. H. Reiff

Department of Space Physics and Astronomy, Rice University

Houston, Texas 77001

M. Smiddy

U. S. Air Force Geophysics Laboratory

Hanscom Air Force Base, Massachusetts 01731

COMPARISON OF MODEL PREDICTIONS WITH DATA FROM SATELLITE S3-2

M. Harel, R. A. Wolf and P. H. Reiff

Space Physics and Astronomy Department, Rice University
Houston, Texas 77001

M. Smiddy

U. S. Air Force Geophysics Laboratory
Hanscom Air Force Base, Massachusetts 01731

Abstract. We have completed a first effort at computer simulating the behavior of the inner magnetosphere during a substorm-type event that occurred on 19 September 1976.

Our computer model simulates many aspects of the behavior of the closed-field-line portion of the earth's magnetosphere, and the auroral and subauroral ionosphere. For these regions, the program self-consistently computes electric fields, electric currents, hot-plasma densities, plasma flow velocities and other parameters.

We present here some highlights of the results of our event simulation. Predicted electric fields for several times during the event agree reasonably well with corresponding data from satellite S3-2. Detailed discussion is presented for a case of rapid subauroral flow that was observed on one S3-2 pass and is predicted by our computer runs. Predictions are made as to the densities of Birkeland currents along the trajectory of satellite S3-2, for three polar-cap passes that occurred during the modeled events. These predictions will be compared directly with magnetometer data from S3-2 for those passes.

Introduction

There has been a longstanding effort at Rice aimed at accurate computer modeling of the earth's inner magnetosphere. Our most recent work is aimed at simulating a specific observed event, using some observations as input to the model and using other observations as tests of model predictions.

In this paper, we shall present some results of our first attempts to model an event, specifically the substorm-type event that had its onset at about 1000 UT on 19 September 1976. This particular substorm was chosen for its "clean" character and wealth of data usable both for input and model testing (Harel *et al.*, 1977). Given certain initial and boundary conditions, the program self-consistently computes electric fields and plasma flow velocities in the ionosphere and equatorial plane, horizontal ionospheric and field-aligned (Birkeland) currents, temperatures and densities of magnetospheric plasma-sheet plasma and other parameters. In this brief paper, we cannot discuss the time histories of all of these parameters through the event. Instead, we present here just some highlights of the results. A much more detailed account will be presented in a future paper (Harel *et al.*, 1979).

The present paper is the latest in a long series of efforts at

self-consistent calculation of electric fields and plasma flows in the coupled magnetosphere-ionosphere system (e.g., Karlson, 1963, 1971; Fejer, 1964; Block, 1966; Vasyliunas, 1970, 1972; Swift, 1971; Mal'tsev, 1974; Wolf, 1970; Jaggi and Wolf, 1973; Wolf, 1974; Harel and Wolf, 1976). This work has gradually progressed over the years to include more physical processes and more realistic boundary conditions. In the last few years, some progress has also been made by attacking the ionospheric and magnetospheric portions of the problem separately. Many detailed ionospheric-current and electric-field distributions have been computed assuming, as input, the distributions of ionospheric conductivities and Birkeland currents (Yasuhara and Akasofu, 1977; Nopper and Carovillano, 1978, 1979, Nisbet et al., 1978; Kamide and Matsushita, 1978). Analogously, the injection of ring-current particles has been studied extensively using assumed, though often time-variable, electric fields; these electric fields have been estimated using semiempirical formulas based on data sets of various kinds and for various time periods (e.g., McIlwain, 1974; Roederer and Hones, 1974; Konradi et al., 1976; Cowley, 1976; Kivelson, 1976; Ejiri et al., 1977, 1978). Our approach has the disadvantage of being more complicated and cumbersome than these alternatives, but it has several advantages. Namely, it includes more physics and fewer questionable boundary conditions, and it potentially can provide a comprehensive view of both ionospheric and magnetospheric aspects of an observed event.

Assumptions and Logic

We attempt to model only the inner magnetosphere, specifically the region where magnetic field lines are certainly closed, available magnetic-field models can be applied with some confidence and plasma-sheet polarization currents are negligible compared with currents due to gradient and curvature drifts. The dynamics of the outer magnetosphere is extremely complicated, and too poorly understood at present for the kind of detailed quantitative modeling that we are attempting. Our choice of modeling region implies an awkward boundary condition, at the boundary between the inner and outer magnetosphere. However, this choice of region allows us to build reasonable models without impractical computing requirements.

Figure 1 shows the basic logic diagram of our model. The basic logical loop (the central pentagon of the figure) is a modification of a diagram given by Vasyliunas (1970).

Let us briefly discuss the diagram, starting with the box labelled "Hot-Particle Distribution." Using a magnetic-field model and assuming isotropic pitch-angle distributions, we can compute gradient-and-curvature drift currents in the magnetosphere. Our magnetic-field model is an Olson-Pfizer (1974) analytic model, but including, in addition, the effects of a time-dependent substorm-current loop. This current loop, including an eastward perturbation current across the tail, a westward electrojet, and connecting Birkeland currents, is a modification of one proposed by McPherron et al. (1973); its current strength was adjusted as suggested by midlatitude magnetograms for the event.

Continuing counterclockwise around the central logical loop in Figure 1, we compute Birkeland-current strengths from the divergence

of the magnetospheric gradient-and-curvature-drift currents, since the magnetization current, while large, is divergence free. Given the Birkeland-current strength, mapped down to the ionosphere, our next step is to derive the potential distribution in the ionosphere. However, to do this, we need two more pieces of input:

(1) the cross-polar-cap potential drop: from S3-2 electric-field data we estimate the potential drop, and assume a simple distribution (basically, a uniform dawn-dusk electric field with a noontime enhancement) at the high-latitude boundary of our calculation. This boundary lies just equatorward of the electric-field-reversal region;

(2) the distribution of ionospheric conductivity: our model Pedersen and Hall conductivities consist of time-dependent terms that include the day-night asymmetry and solar-zenith-angle effect, and a time-dependent term that gives a rough approximation to the auroral conductivity enhancement; in this latter term, the amount of enhancement is adjusted as a function of time in an effort to be consistent with electron fluxes observed from S3-2.

The condition of current conservation in the ionosphere then becomes an elliptic equation in two dimensions, which is solved numerically, given the potential distribution at the polar-cap boundary as one boundary condition and a condition of no current across the low-latitude boundary, which is at approximately 21 geomagnetic latitude.

We map the ionospheric potential distribution out along field lines to the equatorial plane, assuming no field-aligned electric fields, but adding on the induction electric field, to get the total magnetospheric electric field.

We now compute the total drift velocities ($E \times B$, gradient and curvature) of magnetospheric ions and electrons of various energies. Specifically, we compute the motions of the inner edges of plasma-sheet electrons of 5 energies, and ions of 11 energies, each inner edge being represented by approximately 18 independently computed points. The boundary positions are advanced by an amount corresponding to multiplying the computed velocities by the time step t . In computing electron boundary positions, we also include, in an approximate way, the effect of loss by precipitation. For simplicity in these initial model calculations, electrons near the inner edge of the plasma sheet are assumed to be lost by simple strong-pitch-angle scattering, as suggested by Vasyliunas (1968) and Kennel (1969).

The program goes completely around this logical loop every time step, which is typically 30 seconds magnetosphere time.

Figure 2 illustrates some aspects of the event being simulated, which might variously be described as a very long substorm, a quick succession of several short substorms or a substorm followed by a "convection-driven negative bay" (Pytte *et al.*, 1978). The lower panel shows cross-polar-cap potential drops as estimated from S3-2 data. Note that this substorm-type event is associated with an increase in the polar-cap potential drop, an association previously suggested by Mozer (1973). Note also that the potential drop continued to rise after substorm onset, which might account for the prolonged negative bay (Pytte *et al.*, 1978).

Results and Comparison with S3-2 Data

We briefly present here a few highlights of our results, emphasizing some aspects that have been directly compared with observations.

We must emphasize that we are presenting a comparison of observed data with results of our first tries at computer simulating an observed magnetospheric event. Some data were used as input as described in Section II, to help us determine the polar-cap boundary, the cross-polar-cap potential drop, the conductivity and the magnetic-field model, but data were not used in any other significant way. Given the available input data, there is still some flexibility in the boundary conditions, and we could adjust the boundary conditions in various respects to improve agreement with data, but we have not done that yet. Presented below are our first tries at computer simulating the event, with no effort at optimizing the fit.

We have actually done four computer runs, as indicated in Table 1. Run #3 was done with a time-independent magnetic-field model, to isolate the effects of the induction electric field on ring-current injection. The runs also involved two different degrees of latitudinal smoothing of conductivities. (The reason for smoothing of the conductivities is that the difference equation that we use to conserve current in the ionosphere becomes an inaccurate approximation to the differential equation when there are sharp jumps in conductivity. Run #1 involved about as sharp a conductivity gradient as we can handle accurately with the present 21 x 28 grid and present numerical method.) Except for the dotted and dashed curves in Figure 6, all results presented here are for Run #4.

Figures 3-5 show observations vs. theory for the three passes of S3-2 that occurred during the event, before 1300 UT, when the simulation ended. The top two panels of each figure show observed and predicted electric fields. The lower panel shows predicted Birkeland currents. (S3-2 magnetometer data for this date are not reduced yet.) The dotted portion of the top panel represents the polar-cap-and-boundary-layer electric field, which we do not model. However, the input polar-cap potential drop is computed essentially from the area under the dotted curve. The boundary of our calculation (the poleward edge of the computed electric fields), is adjusted in Figures 3-6 (but not Figure 7) to correspond to the observed boundary of the polar-cap-and-boundary-layer region (boundary between dotted and solid observation curves).

We would like to make three general comments concerning the comparison between observed and predicted electric fields in Figures 3-5.

(1) There is little agreement between data and theory with regard to small details, perhaps due to the fact that the model conductivity distribution is smooth and undetailed.

(2) Both data and theory agree that the region below about 60 invariant latitude is rather well shielded from the high-latitude convection field, even in this time-dependent situation. The greatest leakage through the shielding occurred, both in the data and the theory, on the outbound part of pass 4079A South, just after substorm

onset. In the model, auroral conductivities were increased suddenly at onset, and the ring current had not had time to rearrange itself completely to restore strong shielding.

(3) Electric fields on the dawn side generally tend to decline smoothly with decreasing latitude, both in the theory and the data, but the same is not true on the dusk side, where, particularly past 1800 local time, the strongest poleward electric field generally tends to occur well equatorward of the polar-cap boundary. Furthermore, in both the model and S3-2 electric-field data, electric fields below the polar-cap boundary tend to be larger on the dusk side than on the dawn side, an effect previously noticed by Kelley (1976). Our models essentially always show greater potential drops at dusk than at dawn -- a result of Hall currents flowing antisunward across the conductivity jumps at dawn and dusk (Wolf, 1970).

Rapid Subauroral Flow

The most striking feature of the data shown in Figures 3-5 is the sharp electric-field peak observed well below the polar-cap boundary in the last half of orbit 4079B-South (Figure 5). We shall refer to this feature as "rapid subauroral flow." Data from the same auroral-zone pass is shown in more detail in Figure 6 (top panel).

Panels 2-4 display curves for runs 1 (dotted), 2 (dashed), and 4 (solid). Run 3 results are generally similar to run 2 and will not be discussed here.

The second panel of Figure 6 shows calculated electric fields, in a form that displays all the fine structure available in the model. (Our grid spacing is approximately 1.6 in latitude. However, the program employs a special back-correction scheme that allows it to keep track of effects of Birkeland current on a much finer scale. These fine-scale corrections are included in Figure 6, but not Figures 3-5.)

The third panel of Figure 6 shows predicted Birkeland-current strengths along that trajectory.

Panel 4 displays model values of height-integrated Pedersen conductivities. The model global conductivity includes day-night asymmetry, solar-zenith-angle dependence and electron-precipitation effects. The auroral conductivity enhancement is estimated crudely from observed electron fluxes. For a more detailed discussion, see Harel *et al.* (1977). Our computer model cannot tolerate very large conductivity gradients, so we had to smooth the conductivity profile to some extent (see panel 4 and also Table 1).

The bottom panel of Figure 6 shows height-integrated Pedersen conductivity, estimated directly from measured electron fluxes using the formula

$$\Sigma_p \text{ (mho)} = 0.5 + 5.2 \times (\text{Electron energy flux})^{1/2} \quad (1)$$

where the energy flux is in $\text{erg cm}^{-2} \text{ sec}^{-1}$ (Harel *et al.*, 1977). Unfortunately, the geometric factor of the electron detector on S3-2 was too small to allow reliable estimation of the low-latitude edge of the diffuse aurora.

The exciting feature of Figure 6 is, of course, that the computer runs all predicted the observed rapid subauroral flow and at approximately the right location. Similar rapid flows have been

observed many times before, often associated with the trough (Heelis et al., 1976; Smiddy et al., 1977; Maynard, 1978; Spiro et al., 1978).

Note that the location of the peak of the rapid subauroral flow computed in run 4 agrees very well with observations, while the other two runs show peaks that lie approximately a degree poleward of the observed one. This difference in model results is easy to understand physically: for runs 1 and 2 we underestimated the polar-cap potential drop; consequently the plasma-sheet ions were not injected as deep into the magnetosphere as was the case for run 4, and the rapid subauroral flow did not extend to as low latitude (Southwood and Wolf, 1978).

An important feature of our predicted Birkeland currents for this pass (panel 3) is that we get only downward currents. This is different from the observation of an upward current sheet at the poleward edge of one rapid subauroral flow (Smiddy et al., 1977). We attribute this difference to the different local time (2100 MLT) of this earlier measurement. Theoretically, only a single current sheet is needed to account for the peak electric field in the trough region, provided that the conductivity gradient there is large enough (Southwood and Wolf, 1978). Approximately a factor-of-two increase in Pedersen conductivity is needed between 61 and 62 to be consistent with the sharp decline of the observed electric field in that region. The data are not inconsistent with such an increase. Also, the conductivity model with the sharpest gradient (dotted curve) gives rise to the sharpest calculated electric-field peak, as expected.

Our computer model often shows rapid subauroral flows in the dusk-to-midnight sector, though not elsewhere, which is consistent with the previously mentioned observations. We should mention that no other clear rapid subauroral flows were observed during this simulated event, and none are predicted by the model for the S3-2 satellite paths, with the following partial exception: one of the computer runs indicated an electric field on pass 4079A South that peaked at about 42 mV/m and had a shape that would classify it as a marginal case of rapid subauroral flow. The observations indicate, for that case, a complicated structure rather than a clear rapid-subauroral-flow signature.

In the models, we do see multiple reversals of Birkeland currents around local midnight, but we do not see them near dusk. Thus the models always indicate a predominantly downward current in the region of rapid subauroral flow at dusk. On the other hand, the theoretically predicted Birkeland-current reversals at low latitude near midnight may correspond to the effect observed by Smiddy et al. (1977).

We should also acknowledge a different and conflicting interpretation of rapid subauroral flows (Mozer, 1978), an interpretation in terms of field-aligned potential drops between relevant satellite altitudes (250-1500 km) and the lower ionosphere.

Summary

We have displayed some highlights of results of our first attempt at simulating an observed magnetospheric event. Comparison with observations has come out remarkably well, particularly considering

that, in these first tries, we have not adjusted any boundary conditions or assumptions to improve agreement with the data. Of course, much work remains to be done to include more physics in the models and to model more and different events.

Acknowledgments. We are grateful to Ameen Ahmad, H. Kent Hills, Janice Karty, and Robert Spiro for their work in displaying model results, to W. J. Burke, D. A. Hardy and F. J. Rich for their efforts in reducing data from the S3-2 satellite, and to Robert Spiro for several illuminating discussions and for helpful comments on the manuscript, which is based on the paper presented at the Chapman Conference on Quantitative Modeling of Magnetospheric Processes. Our work at analyzing and interpreting data from satellite S3-2 is supported primarily by U.S. Air Force Contract F19628-78-C-0078. Other aspects and applications of the computer simulation effort are supported by U.S. Air Force Grant F19628-77-C-0005, by National Science Foundation grant ATM74-21185, and by NASA grants NGR 44-006-137 and NGL44-006-012.

References

- Block, L. P., On the distribution of electric fields in the magnetosphere, J. Geophys. Res., 71, 855, 1966.
- Cowley, S. W. H., Energy transport and diffusion, in Physics of Solar Planetary Environments, ed. D. J. Williams, Amer. Geophys. Un., Washington, D.C., p. 582, 1976.
- Ejiri, M., R. A. Hoffman and P. H. Smith, Energetic particle penetrations into the inner magnetosphere, Goddard Space Flight Center Report X-625-77-254, 1977
- Ejiri, M., R. A. Hoffman and P. H. Smith, The convection electric field model for the magnetosphere based on Explorer 45 observations, J. Geophys. Res., 83, 4811, 1978
- Fejer, J.A., Theory of geomagnetic daily disturbance variations, J. Geophys. Res., 69, 123, 1964.
- Harel, M., and R. A. Wolf, Convection, in Physics of Solar-Planetary Environments, Vol. II, edited by D. J. Williams, Amer. Geophys. Un., Washington, D. C., p. 617, 1976.
- Harel, M., R. A. Wolf, P. H. Reiff and H. K. Hills, Study of plasma flow near the earth's plasmapause, U.S. Air Force Geophysics Laboratory Report AFGL - TR-77-0286, 1977.
- Harel, M., R. A. Wolf, P. H. Reiff, R. W. Spiro, H. K. Hills, M. Smiddy W. J. Burke and F. J. Rich, in preparation, 1979.
- Heelis, R. A., R. W. Spiro, W. B. Hanson and J. L. Burch, Magnetosphere-ionosphere coupling in the mid-latitude trough, Trans. Am. Geophys. Union, 57, 990, 1976.
- Jaggi, R. K. and R. A. Wolf, Self-consistent calculation of the motion of a sheet of ions in the magnetosphere, J. Geophys. Res., 78, 2852, 1973.
- Kamide, Y. and S. Matsushita, Simulation studies of ionospheric electric fields and currents in relation to field-aligned currents. 1. Quiet periods, submitted to J. Geophys. Res., 1978.
- Karlson, E. T., Streaming of plasma through a magnetic dipole field, Phys. Fluids, 6, 708, 1963.
- Karlson, E. T., Plasma flow in the magnetosphere. I. A two-dimensional model of stationary flow, Cosm. Electrodyn., 1 474, 1971.
- Kelley, M. C., Evidence that auroral-zone electric fields act in opposition to super-rotation of the upper atmosphere, Planet Space Sci., 24, 355, 1976.
- Kennel, C. F., Consequences of a magnetospheric plasma, Rev. Geophys. 7, 379, 1969.
- Kivelson, M. G., Magnetospheric electric fields and their variation with geomagnetic activity, Rev. Geophys. Space Phys., 14, 189, 1976.
- Konradi, A., C. L. Semar, and T. A. Fritz, Injection boundary dynamics during a geomagnetic storm, J. Geophys. Res., 81, 3851, 1976.
- Mal'tsev, Yu. P., The effect of ionospheric conductivity on the convection system in the magnetosphere, Geomag. Aeron., 4, 128, 1974.
- Maynard, N. C., On large poleward-directed electric fields at sub-auroral latitudes, Geophys. Res. Lett., 5, 617, 1978.
- McIlwain, C. E., Substorm injection boundaries, in Magnetospheric Physics, edited by B. M. McCormac, D. Reidel, Dordrecht-Holland, p. 143, 1974.

- McPherron, R. L., C. T. Russell and M. P. Aubry, Satellite studies of magnetospheric substorms on August 15, 1968. 9. Phenomenological model of substorms, J. Geophys. Res., 78, 3131, 1973.
- Mozer, F. S., On the relationship between the growth and expansion phases of substorms and magnetospheric convection, J. Geophys. Res., 78, 1719, 1973.
- Mozer, F. S., Implications of S3-3 and ISEE electric field data on models of magnetospheric electric fields, paper presented at the Chapman Conference on Quantitative Modeling of Magnetospheric Processes, La Jolla, Ca., 1978.
- Nisbet, J. S., M. J. Miller and L. A. Carpenter, Currents and electric fields in the ionosphere due to field-aligned auroral currents, J. Geophys. Res., 83, 2647, 1978.
- Nopper, R. W. Jr., and R. L. Carovillano, Polar equatorial coupling during magnetically active periods, Geophys. Res. Lett., 5, 699, 1978.
- Nopper, R. W. Jr., and R. L. Carovillano, Ionospheric electric fields driven by field-aligned currents, in Quantitative Modeling of the Magnetospheric Processes, Geophys. Monogr. Soc., Vol. 21, edited by W. P. Olson, AGU, Washington, D. C., 1979.
- Olson, W. P., and K. A. Pfitzer, A quantitative model of the magnetospheric magnetic field, J. Geophys. Res., 79, 3739, 1974.
- Pytte, T. R., R. L. McPherron, E. W. Hones, Jr., and H. I. West, Jr., Multiple-satellite studies of magnetospheric substorms: distinction between polar magnetic substorms and convection-driven negative bays, J. Geophys. Res., 83, 663, 1978.
- Roederer, J. G., and E. W. Hones, Jr., Motion of magnetospheric particle clouds in a time-dependent electric field model, J. Geophys. Res., 79, 1432, 1974.
- Smiddy, M., M. Kelley, W. Burke, F. Rich, R. S. Sagalyn, B. Schumann, R. Hays and S. Lai, Intense poleward-directed electric fields near the ionospheric projection of the plasmopause, Geophys. Res. Lett., 4, 543, 1977.
- Smith, P. H., H. K. Bewtra and R. A. Hoffman, Motions of charged particles in the magnetosphere under the influence of a time-varying large-scale convection electric field, in Quantitative Modeling of the Magnetospheric Processes, Geophys. Monogr. Ser., vol. 21, edited by W. P. Olson, AGU, Washington, D.C., 1979.
- Southwood, D. J., and R. A. Wolf, An assessment of the role of precipitation in magnetospheric convection, J. Geophys. Res., 83, 5227, 1978.
- Spiro, R. W., R. A. Heelis and W. B. Hanson, Ion convection and the formation of the midlatitude F-region ionospheric trough, J. Geophys. Res., 83, 4255, 1978.
- Swift, D. W., Possible mechanisms for formation of the ring current belt, J. Geophys. Res., 76, 2276, 1971.
- Vasyliunas, V. M., A mathematical model of plasma motions in the magnetosphere, Trans. Am. Geophys. Un., 49, 232, 1968.
- Vasyliunas, V. M., Mathematical models of magnetospheric convection and its coupling to the ionosphere, in Particles and Fields in the Magnetosphere, edited by B. M. McCormac, D. Reidel, Dordrecht-Holland, p. 60, 1970.
- Vasyliunas, V. M., The interrelationship of magnetospheric processes, in Earth's Magnetospheric Processes, edited by B. M. McCormac, D. Reidel, Dordrecht-Holland, p. 29, 1972.

- Wolf, R. A., Effects of ionospheric conductivity on convective flow of plasma in the magnetosphere, J. Geophys. Res., 75, 4677, 1970.
- Wolf, R. A., Calculations of magnetospheric electric fields, in Magnetospheric Physics, edited by B. M. McCormac, D. Reidel, Dordrecht-Holland, p. 167, 1974.
- Yasuhara, F. and S. -I. Akasofu, Field-aligned currents and ionospheric electric fields, J. Geophys. Res., 82, 1279, 1977.

Figure Captions

Fig. 1. Overall logic diagram for our program. The central pentagon represents the main computational loop, executed every time step. The rectangles that appear at the corners of the pentagon represent basic parameters computed. Input data are indicated by curly brackets. Subsidiary models, used as input to the main program, are indicated by rectangles with rounded corners. Dashed lines indicate features that we plan to include in the program but have not included yet

Fig. 2. Fort Churchill H-magnetogram and polar-cap potential drop for 19 September 1976. The lower panel shows polar-cap potential drops estimated from S3-2 electric-field data. Sizes of boxes are indicative of estimated errors. The solid curve shows the potential drop assumed in the simulation. Electric-field data from the 1140 UT pass arrived later than those from the other passes, and as a result some simulation runs followed the dashed line from 1040 to 1300 UT.

Fig. 3. Data and theory for the 1000 UT pass of satellite S3-2. The top panel shows data from the AFGL electric field instrument. We have plotted the forward component of E, i.e., the component in the direction of satellite motion. The dotted section of the curve is the polar-cap-and-boundary-layer region, which we do not model. The second panel shows the corresponding component of the theoretically predicted electric field at the satellite's location (latitude, longitude and altitude) for the universal times in question. The bottom panel shows predicted Birkeland-current strength (positive values mean upward current). The legend gives Greenwich Mean Time, magnetic local time and invariant latitude. Satellite altitude ranges from 1025 km to 1375 km.

Fig. 4. Data and theory for the 1050 UT pass of S3-2. The format is the same as Figure 3. Satellite altitude ranges from 800 km to 260 km.

Fig. 5. Data and theory for 1140 UT pass of S3-2. The format is the same as Figure 3. Satellite altitude ranges from 1000 km to 1360 km.

Fig. 6. Detailed view of the dusk-auroral-zone pass for the southern part of orbit 4079B of satellite S3-2. The top panel shows the observed electric-field component opposite to satellite motion (approximately the poleward component). The second panel gives essentially the same component of the theoretical-model electric field. The third panel gives predicted Birkeland currents, and the fourth panel shows the model height-integrated Pedersen conductivities. Solid curves in panels 2-4 pertain to the same computer run as in Figures 3-5; the dotted and dashed curves correspond to lower polar-cap potential drops, the dotted lines one to a less-smearred conductivity model. The bottom panel shows conductivities estimated directly from the data using equation (1).

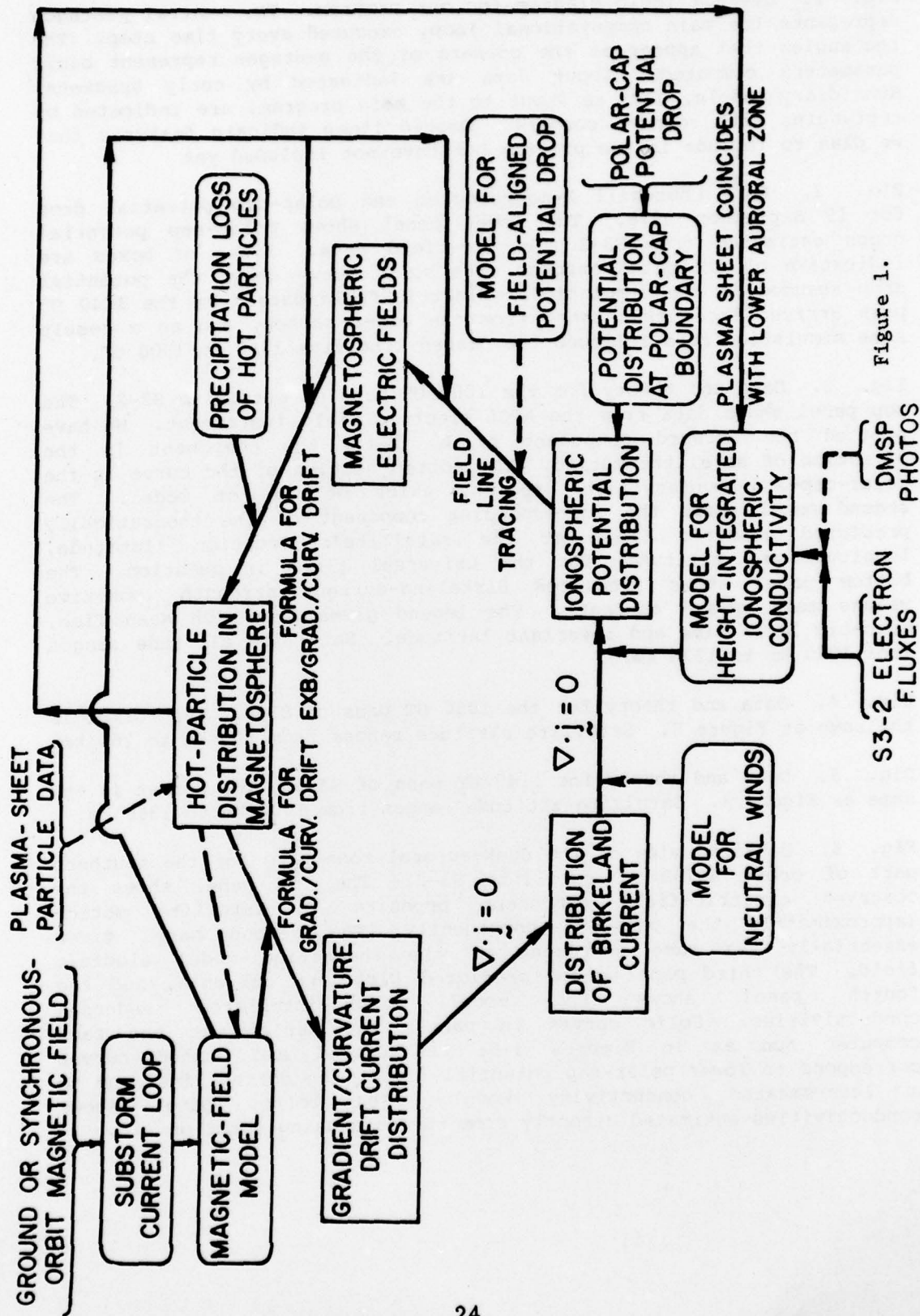


Figure 1.

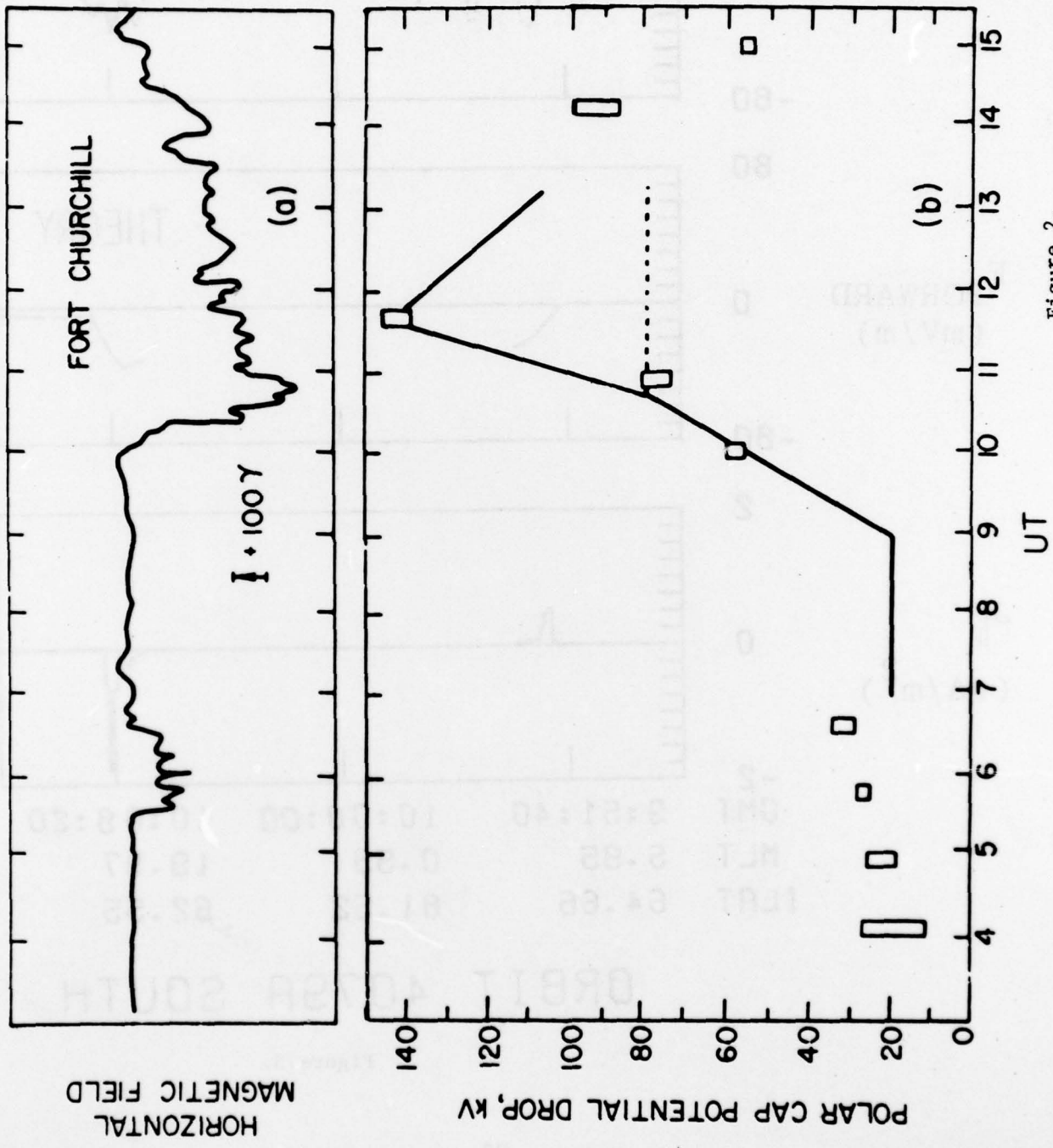
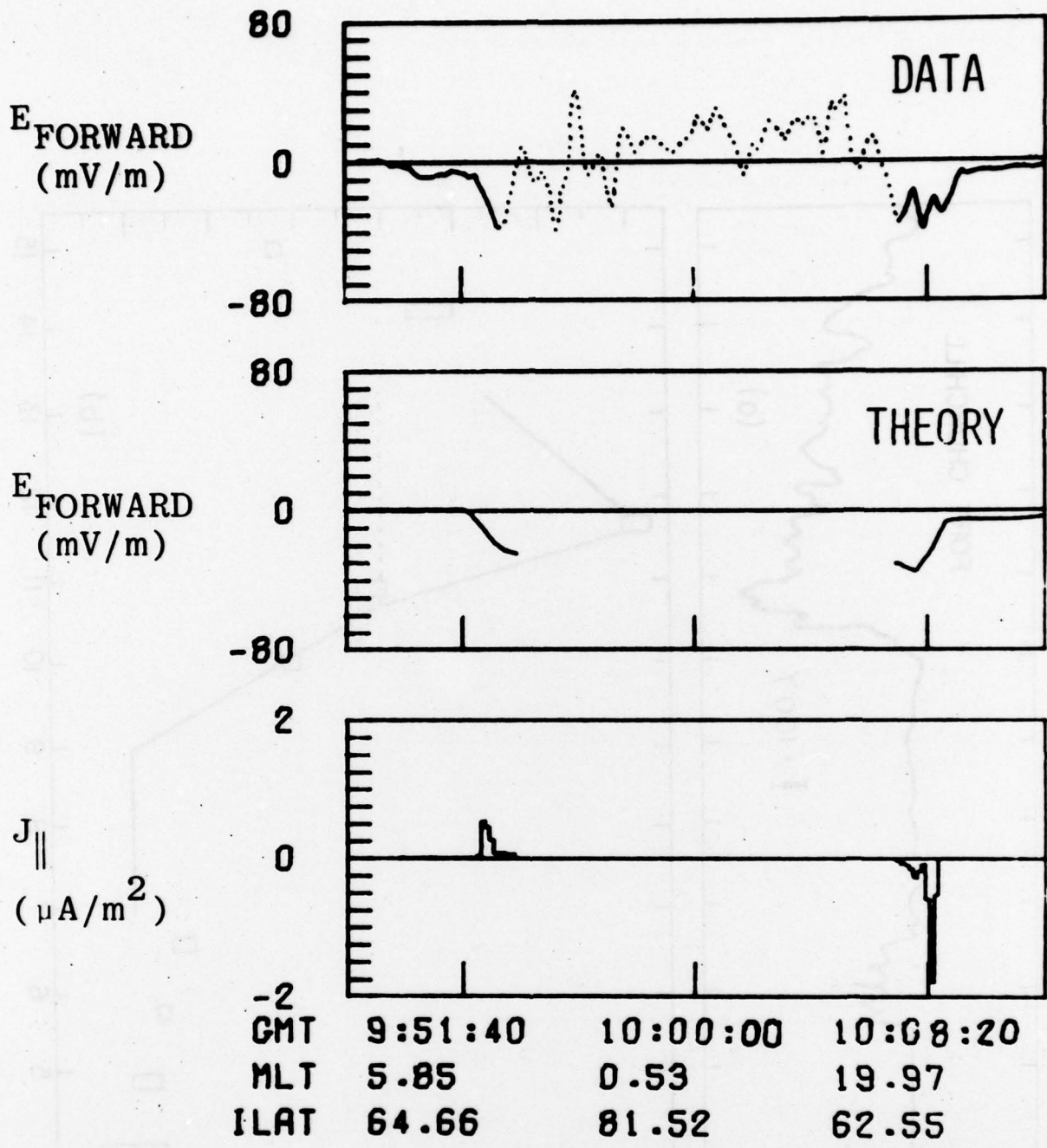
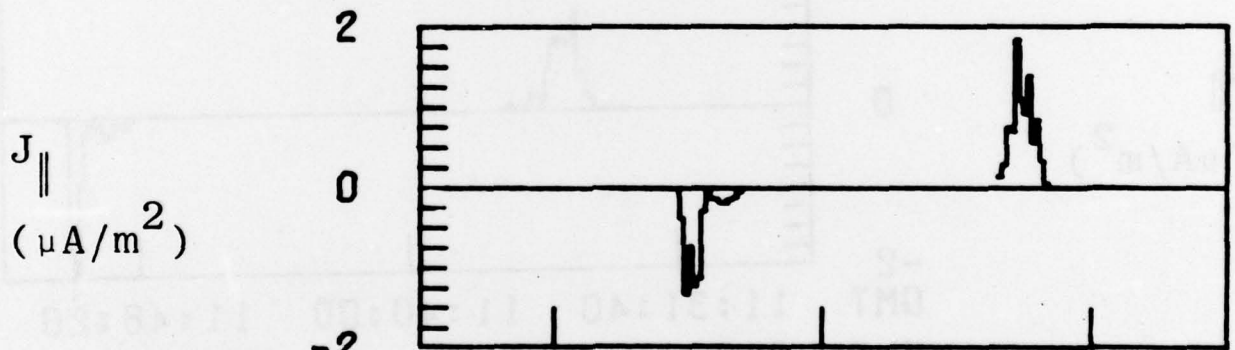
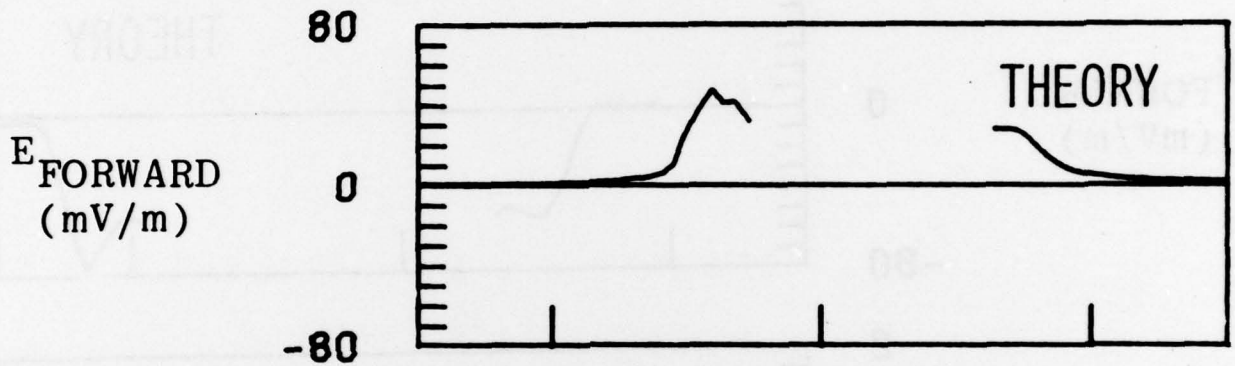
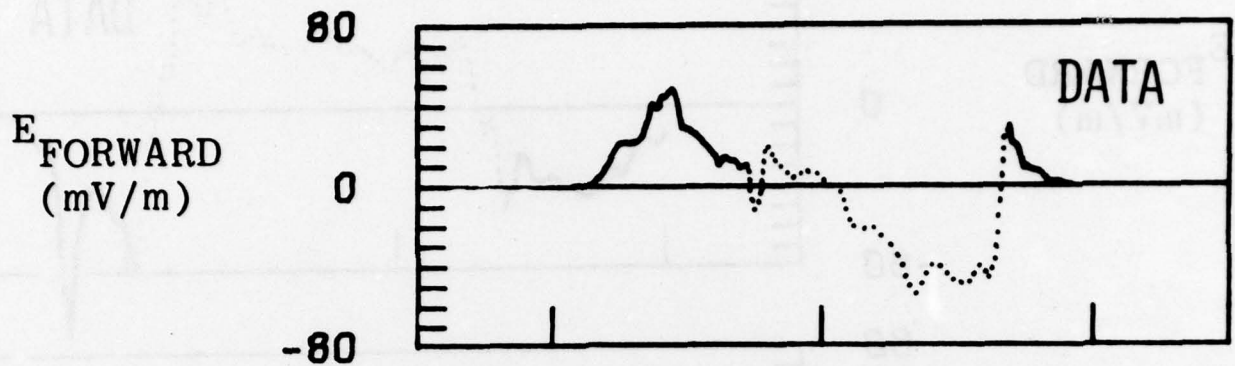


Figure 2.



ORBIT 4079A SOUTH

Figure 3.

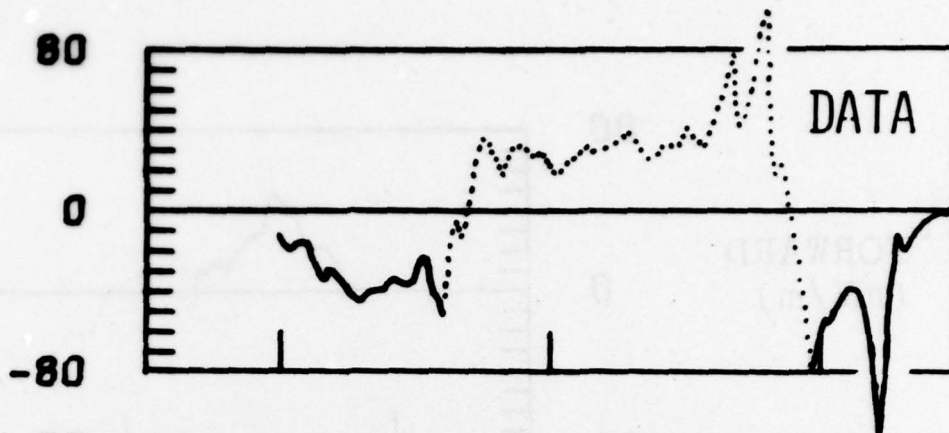


GMT	10:41:40	10:50:00	10:58:20
MLT	18.44	15.09	8.64
ILAT	54.48	79.32	62.76

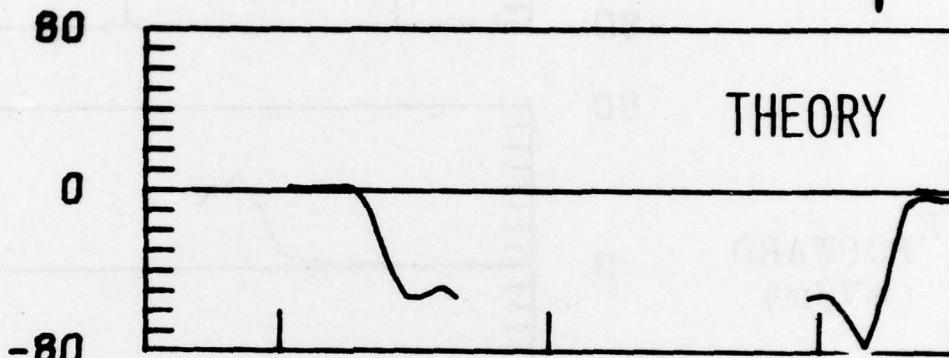
ORBIT 4079A NORTH

Figure 4.

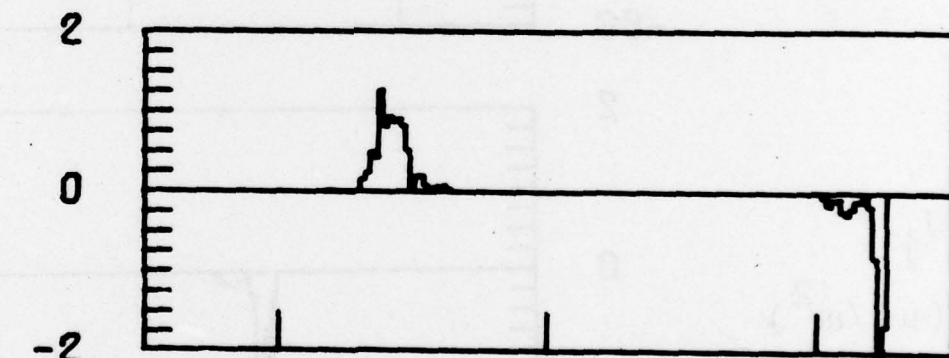
E_{FORWARD}
(mV/m)



E_{FORWARD}
(mV/m)



J_{\parallel}
($\mu\text{A}/\text{m}^2$)



GMT	11:31:40	11:40:00	11:48:20
MLT	6.84	3.92	19.27
ILAT	63.07	87.28	66.68

ORBIT 4079B SOUTH

Figure 5.

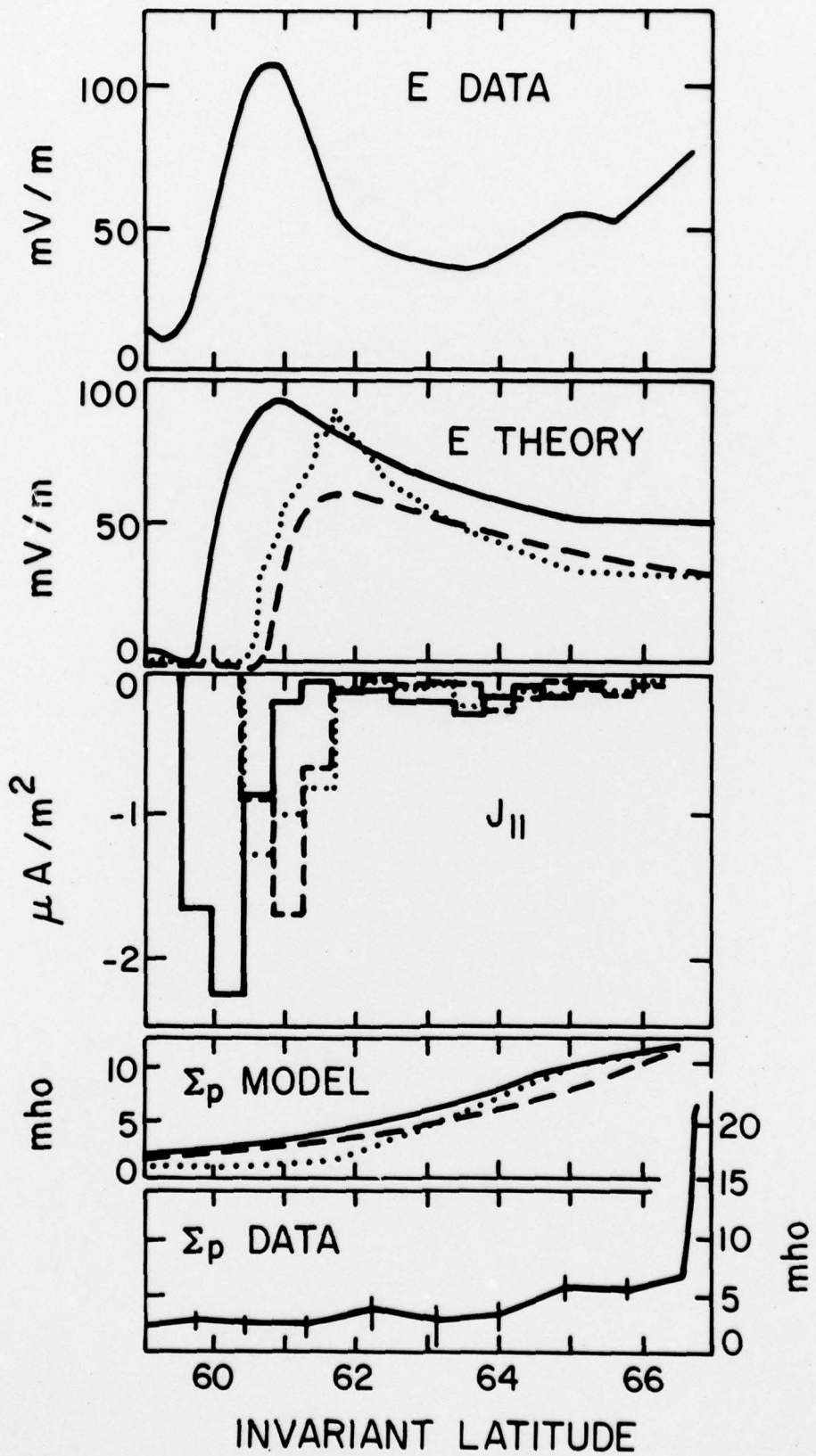


Figure 6. 29